water

MDPI

Article

Study of Seepage Laws of Deep Rock Mass Under Different Water Temperatures Based on Porous Media

Heming Qiu, Shuyun Zhu *, Han Fang and Xiangcheng Lu

School of Resources and Geosciences, China University of Mining and Technology, Xuzhou 221116, China; ts23010135p31@cumt.edu.cn (H.Q.); geohanfang@163.com (H.F.); 18560520915@163.com (X.L.)
* Correspondence: shyzhuqiao@163.com

Abstract: Deep coal mining is faced with high temperature, high seepage pressure, and high ground stress, and there is a complex nonlinear coupling relationship between the temperature of water in deep rock mass and its seepage. Based on the background of deep mining in Zhaolou Coal Mine in Shandong Province, China, the hydraulic conductivity of artificial rock samples with similar materials was tested indoors under different water temperatures of 30~80 °C. On the basis of deep rock samples collected in the field, the hydraulic conductivity has a nonlinear positive correlation with the rise of water temperature. The difference in hydraulic conductivity at the highest and lowest temperatures is two to three times. By means of multi-physics coupling finite element software (COMSOL Multiphysics, COMSOL Inc., Stockholm, Sweden), combined with the actual geological background, the regularity was found to be consistent with the laboratory experiment and further proves that the inlet pressure has no effect on the hydraulic conductivity. Subsequent analyses revealed that the influence of temperature on the seepage field is mainly reflected in the change of fluid kinematic viscosity with temperature, which causes the change in the hydraulic conductivity. According to the formula, the hydraulic conductivity of the rock at 80 °C is 2.31 times higher than its hydraulic conductivity at 30 °C, which is matched by the indoor test results. The engineering performance is that as the temperature of the deep rock body increases, the ability of water to penetrate rocks increases, and the water inflow of the working face increases. The results can be applied to the prevention of water hazard threats in deep coal mining.

Keywords: deep rock mass; hydraulic conductivity; water temperature; laboratory experiment; kinematic viscosity

check for updates

Academic Editor: Fernando António Leal Pacheco

Received: 11 December 2024
Revised: 19 January 2025
Accepted: 22 January 2025
Published: 27 January 2025

Citation: Qiu, H.; Zhu, S.; Fang, H.; Lu, X. Study of Seepage Laws of Deep Rock Mass Under Different Water Temperatures Based on Porous Media. *Water* **2025**, *17*, 357. https://doi.org/10.3390/w17030357

Copyright: © 2025 by the authors. Licensee MDPI, Basel, Switzerland. This article is an open access article distributed under the terms and conditions of the Creative Commons Attribution (CC BY) license (https://creativecommons.org/licenses/by/4.0/).

1. Introduction

With the exploitation and utilization of shallow underground space and the exhaustion of mineral resources, human activities and the exploitation of resources have extended into deep spaces [1,2]. Compared with shallow rock mass, deep rock mass has characteristics of high ground stress, high osmotic pressure, and high temperatures [3,4]; the interaction of these three factors on deep rock mass is complex, and the study of their coupling effects is extremely important for the development and utilization of deep resources. Scholars have gradually studied the effect of coupling on rock properties. The coupling of permeability and mechanics [5–7] and the coupling of permeability and heat transfer [8–10] are important research directions. Ji et al. [11] proposed a method of rock engineering system to analyze the coupling mechanism of seepage stress in the coal seam floor, and Pan et al. [12] used the hydraulic-thermal coupling program FRHT3D and applied it to rock mass engineering

practice. The coupling effect of the three factors has also been noticed by many scholars, and related studies have been carried out. Yan et al. [13] simulated rock cracking driven by multiple physical fields using the finite-discrete element method (FDEM). Based on heat transfer theory, seepage mechanics, and elastoplastic mechanics, Ji et al. [14] established a mathematical model in which the coupling of seepage, stress, and heat transfer in heat recovery was established.

Many research methods and models have been proposed to study the coupling in rock mass. The mathematical method and its solution have provided a theoretical basis for the implementation of laboratory experiments and numerical simulations. Laboratory experimentation [7,15] has good reliability and practical significance for the study of coupling effects. Shi et al. [16] studied the nonlinear effect of fracture length on rock permeability through laboratory experiments, and Wang et al. [17] analyzed the influence of mining on the seepage of the ascending dewatering well through laboratory sand-tank experiments. Numerical models can effectively characterize the effects of seepage field evolution, heat transfer processes, and mechanical response coupling on rock mass [18,19] and is widely used to verify mathematical solution results and laboratory experimental results [20,21]. Li et al. [22] verified the water inrush model of a strong water-conducting collapse column through coupled cloud images generated by numerical simulation software, and Teng et al. [23] developed an effective permeability model and carried out experimental verification and full-coupling numerical simulation to explain the relationship between rock permeability and deformation.

In addition, many scholars have studied the hydraulic conductivity of rock and soil. Laboratory experiments by M M Khlapuk et al. [24] on filtration using Darcy's facility reveal patterns of the hydraulic gradient's influence on the hydraulic conductivity in soils with different particle size distributions. Based on the research results for selected model soils, the dependence of hydraulic conductivity on the magnitude of the hydraulic gradient was established. Hydraulic conductivity increases with an increase in the hydraulic gradient. Esra Güneri et al. [25], in order to improve the engineering behavior of soils under high temperatures using thermally durable materials, investigated volume deformation and hydraulic conductivity behavior of 30% bentonite–70% sand mixtures in the presence of fiberglass additives. The hydraulic conductivity increased under high temperatures with the fiberglass additive.

However, due to the limitations of the indoor model test, some complex conditions are difficult to achieve, and some phenomena or data are difficult to directly measure; numerical simulation can directly observe the parameters, but using only numerical simulation, it will be difficult to measure accuracy. Therefore, this paper combines the two and carries out a further study on the basis of the actual test.

The first mining level of Zhaolou Coal Mine in Shandong Province of China is −860 m, the buried depth of the coal seam reaches 700~1200 m, the rock temperature is 40–50 °C, and the average water temperature is about 42 °C, which is a typical deep mining mine. Based on the background of deep mining in Zhaolou Coal Mine, this paper analyzes the interaction between the temperature field and seepage field of deep rock mass by means of laboratory experimentation and coupled numerical simulation on the basis of considering thermal conductivity and permeability. Changes in water inflow caused by a change in the hydraulic conductivity of a deep aquifer under the background of mining is an important reason for the occurrence of water inrush disaster [26]. This paper mainly considers variations in hydraulic conductivity under the condition of changing water temperature, and the insights from this study have a good reference significance for the prevention and control of mine water disasters and the exploitation of deep resources.

2. Methods

2.1. Sample Preparation

Due to the small hydraulic conductivity of natural rocks, it is difficult to conduct indoor permeability experiments, and artificial large fractures in rocks are widely adopted [27]. Porous media were used in this paper to obtain relevant experimental parameters, on the basis of keeping the porosity and particle size ratio of artificial rocks and natural rocks approximately the same. By changing the water–cement ratio of the simulated material (sand, cement, and water), the rock hydraulic conductivity was amplified so as to ensure the normal conduct of the experiment without seriously affecting the experimental results. In the selection of simulated materials, the sand was filtered by sieve method from river sand (particle size was about 0.1–0.2 mm), the cement was ordinary Portland cement, and the sample was prepared. By adjusting the water-cement ratios of different rock samples, which were X:1:1, X:1:1.2, X:1.5:1 (X being 3, 4, and 5), fine sandstones with different cementation degrees and different sand content were simulated so as to obtain the permeability changes of various sandstones at different temperatures. Three sets of rock samples with different water–cement ratios are shown in Figure 1. To accurately obtain the experimental results, the diameter of the samples was 75 mm and the length 150 mm, and they were dried for 7 days after sample formation for the experiment. To establish a similar connection between the artificial rock samples and the natural rocks, rock core obtained from drilling of the 5301 working face of Zhaolou Coal Mine was used, and rock with the lithology of fine sandstone was selected to make standard samples with a diameter of 75 mm and a length of 150 mm. Four rock samples were made (Table 1).



Figure 1. Similar rock samples.

To establish the connection between the artificial rock samples and the actual site rocks (original), the internal structure, physical and mechanical properties, porosity and other aspects were analyzed, and the connection model between the rock sample and the original was established by comparing the similarities and differences.

Wave velocity testing is a way to reflect the internal density of the samples. According to the physical properties of the wave, the wave travels fastest in solids, followed by liquids, and the slowest in gas. Therefore, the denser the sample, the higher the corresponding P-wave velocity will be.

Porosity is one of the important characteristics of rocks. It represents the ratio of the volume occupied by the pores inside the rock to the overall volume of the rock and can also reflect the physical properties of many rocks. There are many methods for testing porosity.

To combine the relevant experimental results, this experiment intended to test the porosity of the rock sample fragments after the compressive strength experiment, and two methods were adopted. They were the saturated drainage method at a normal temperature and the saturated drainage method at a high temperature, respectively. The saturated drainage method refers to the comparison of the dry weight of the rock samples and the wet weight of the saturated rock samples after a long time soaking; the difference is the quality of the pore water inside the rock samples. The volume of internal pores is translated from the density of water, with porosity $\mathcal{E}$ = V water/V total × 100%.

Table 1. Wave velocity test results and porosity of artificial and field rock samples.

Scheme 30	Ratio (Sand:Cement:Water) /Rock Numbering	Simulated Rock/Lithology	Wave Velocity	Porosity (30 °C)	Porosity (80 °C)
Artificial rock samples	3:1:1	Fine sandstone	2045.62	26.53%	28.57%
	4:1:1	Fine sandstone	1966.48	28.50%	29.73%
	5:1:1	Fine sandstone	1403.34	30.68%	31.55%
	3:1.5:1	Fine sandstone	2428.17	20.92%	22.68%
	4:1.5:1	Fine sandstone	2288.59	21.58%	24.01%
	5:1.5:1	Fine sandstone	2259.01	22.75%	28.53%
Field rock samples	1	Fine sandstone	2747.37	0.40%	0.44%
	2	Fine sandstone	2953.06	1.01%	1.52%
	3	Fine sandstone	2451.75	6.55%	8.05%
	4	Fine sandstone	2513.46	Disintegration	Disintegration

According to the wave velocity test and porosity results of the artificial rock samples and field rock samples (Table 1), the wave velocity of fine sandstones simulated by fine sand material is very close to that of the original fine sandstone. According to the rate distribution of rock samples made of similar materials, the number of internal pores in the rock samples increases, and the longitudinal wave passing time becomes longer during the cementation process due to the increase in sand content; the speed also showed a downward trend. By comparing the rock samples with different cementation degrees, it can be seen that the rate of the rock samples with a high cementation degree (X:1.5:1) is significantly higher than that of the group with (X:1:1), indicating that the internal density of the rock samples with a high cementation degree is higher than that of the rock samples with a low cementation degree. According to the experimental results, the rock sample rate of 3:1.5:1 is the closest to that of fine sandstone, and the difference is less than 10%. The similarity of this simulation is more than 90% without considering other physical and mechanical properties, and the rock samples are very close to the original internal structural density.

2.2. Experimental Apparatus

A self-made large-scale permeability testing apparatus (Figure 2) was used in the experiment. A specially sealed steel tank with a size of 200 mm long and a diameter of 85 mm was used. The rock samples were placed in the tank, and a small amount of non-shrinkage cement was used to fill the gap between the rock sample and the tank wall, which was allowed to dry for 2–3 days before being used in the experiment. The rock samples were sealed in the tank with non-shrinkage cement and were dried for a further 2–3 days before being used in the experiment. A flange was designed for each inlet and outlet wherein a water inlet was arranged in the middle of the upper flange and was connected with a high-pressure pipe to the pressure pump. A water outlet was arranged in the middle of the lower flange and was connected with a high-pressure rubber pipe to

the pallet balance. The steel tank device (number 8 in the figure) encapsulating the rock sample was immersed in a tank of water, and the rock sample was completely isolated from the water in the tank. A temperature heating apparatus was set up below to maintain the required temperature, and a thermometer was placed in the water to collect real-time temperature data and adjust the heating intensity in time. A pressure gauge was placed at each inlet and outlet, and after the pressure and temperature stabilized, the water inflow into the receiver on the electronic balance within the unit time period was tested. The water in the water bucket was heated to the corresponding temperature in advance.

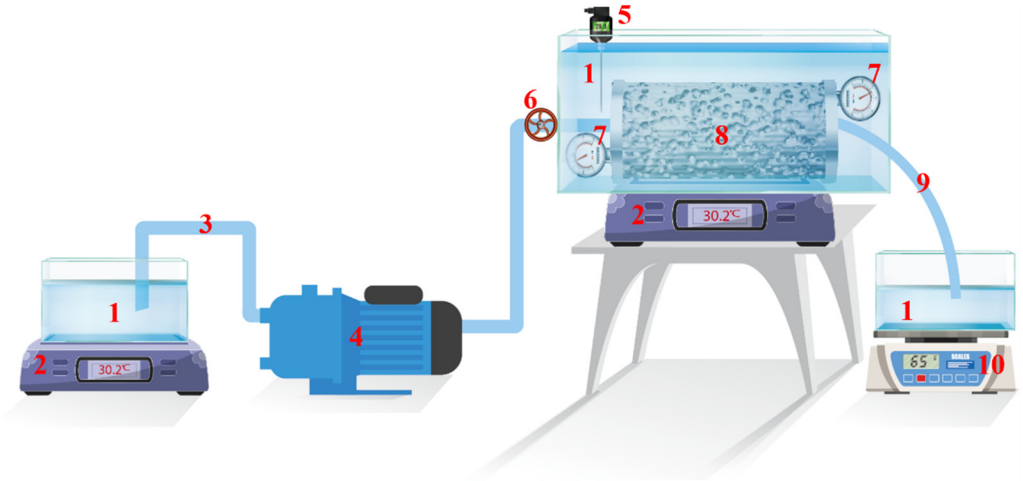

Figure 2. Experimental apparatus for measuring hydraulic conductivity of rock samples with variable water temperature. 1—Water bucket, 2—Heating apparatus, 3—High-pressure pipe, 4—Pressure pump, 5—Thermometer, 6—Valve, 7—Pressure gauge, 8—Rock samples equipment, 9—High-pressure rubber pipe, 10—Electronic balance.

2.3. Selection of Calculation Formula of Hydraulic Conductivity

In isotropic continuous porous media, the unit flow rate under a unit hydraulic gradient is the hydraulic conductivity, which represents the difficulty of fluid penetrating through porous rock. The rock samples used in the experiment are regarded as rock mass dominated by pore structure; therefore, Darcy's law [28] is still chosen as the basic principle for the apparatus to test, analyze, and calculate the hydraulic conductivity of rock samples, and its classic expression is as follows:

$$Q = KA\frac{\Delta h}{l} = KAi \tag{1}$$

$$V = \frac{Q}{A} = Ki \tag{2}$$

where $\frac{\Delta h}{l}$ refers to hydraulic gradient i, A is the water crossing section area (m^2), K is the hydraulic conductivity (m/s), Q is the seepage water quantity per unit time (m^3/s), and V is the seepage velocity (m/s).

According to the known data, the diameter of the rock samples is 75 mm, the length is 150 mm, and the water inflow Q per unit time can be measured by the electronic balance; Darcy's law is used to calculate the hydraulic conductivity of the rock samples.

2.4. Model Establishment

This numerical simulation is the verification of the laboratory experiment; the real rock sample parameters obtained from field sampling were combined with the laboratory exper-

iment, and the change in hydraulic conductivity of the porous media sandstones under the condition of variable water temperature is reflected through numerical simulation.

According to the actual geological conditions, in the 5301 working face of Zhaolou Coal Mine, where the research area is located, the coal seam being exploited is the No. 3 coal seam of the Shanxi Formation of the Permian system, and the top and bottom of the No. 3 coal seam are sandstone, which is also the direct aquifer of the coal seam. After measurement, the values of various calculation parameters are shown in Table 2, where the density $f(T)$ and dynamic viscosity (Figure 3) of water are set as empirical functions of temperature. The properties of rock mass are basically unchanged at low temperatures, and the permeability of rock mass is set to a fixed value for the convenience of research.

$$f(T) = -0.0055T^2 + 0.0228T + 999.99 \quad (3)$$

Table 2. Calculation parameters of numerical simulation.

Attributes	Specific Heat ($\frac{kJ}{m^3}$)	Density ($\frac{Kg}{m^3}$)	Permeability (m^2)	Coefficient of Heat Conduction ($\frac{w}{m}$·k)	Porosity (%)	Dynamic Viscosity (Pa·s)
Rock	2190	2700	5×10^{-10}	3.1	15	-
Water	4190	f(T)	-	0.6	-	$\mu(T)$

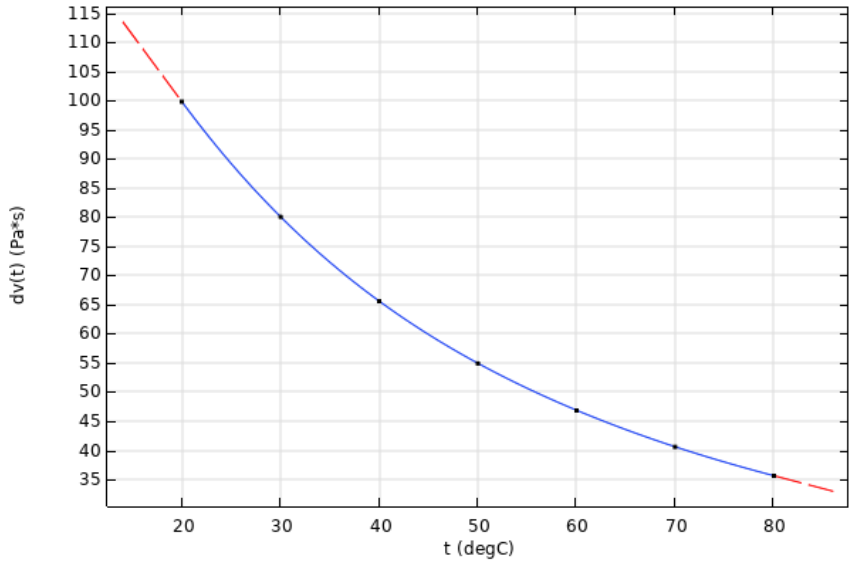

Figure 3. Empirical relationship between dynamic viscosity and temperature.

The prototype of the 3D model is a 150 mm × 75 mm cylindrical rock. Water flows in from the left side of the rock and flows out from the right side. The surrounding area is sealed by concrete, and only the seepage inlet and outlet surfaces are retained. The schematic of the model is shown in Figure 4. The inlet pressure was applied at different temperatures to observe the changes in percolation parameters. The rock is considered to be a homogeneous porous media, the reference rock is sandstone, and the physical fields selected are Darcy seepage and porous media heat transfer module. The experimental temperature was selected to be 30–80 °C, regardless of the changes in the rock mass skeleton and solid particles under the influence of temperature. According to the experimental model, the upper and lower boundaries were set as impermeable boundaries; the left boundary was the pressure boundary entrance, and the right side was the exit. According to the experimental model, the rock as a whole was immersed in hot water, so there was a

variable temperature boundary around it, and the boundary at the outlet was not in contact with hot water. The normal temperature boundary was set at 20 °C, and the duration of this simulation was set at 600 min for full heating. The porous media is isotropic, so to observe the changes in the relevant seepage parameters, the central point of the entire core was selected as the monitoring point (X: 75 mm, Y: 0 mm, and Z: 0 mm) (Figure 4), and the tangential hydraulic conductivity and Darcy velocity changes with the inlet temperature and pressure were observed.

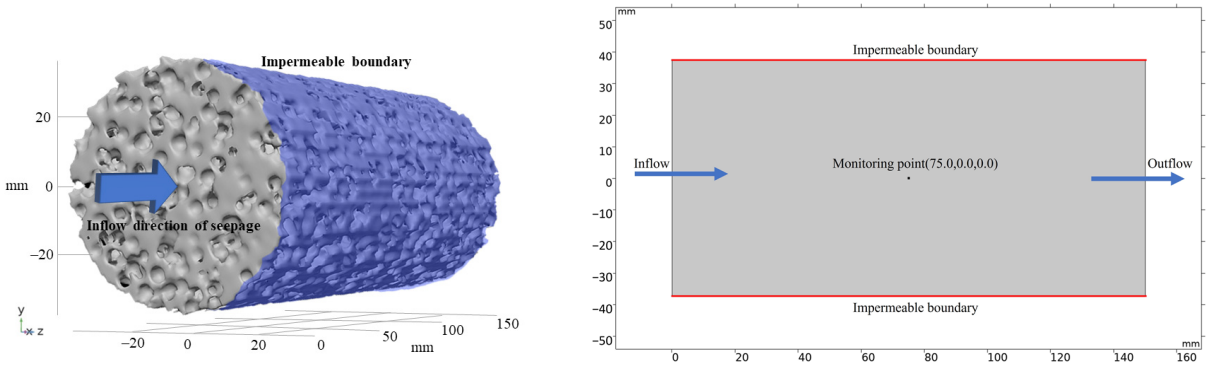

Figure 4. Numerical model of the penetration experiment.

3. Results of Laboratory Experiment

3.1. Experimental Results of Rock Samples with Porous Media

According to the preset ratio, the hydraulic conductivity of the three groups of rock samples (with ratios of X:1:1, X:1:1.2, and X:1.5:1) was tested at different temperatures, respectively, under inlet pressures of 0.6 MPa, 1.0 MPa, and 1.4 MPa, and the variety graphs of the hydraulic conductivity with temperature were obtained (Figures 5–7). The rock sample with 3:1:1.2 ratio was not obtained due to its low permeability during the laboratory experiment, and the rock sample with 3:1.5:1 ratio was not obtained due to its low water pressure permeability at 0.6 MPa. Moreover, to make longitudinal comparisons between the three groups of rock samples, rock samples of different ratios (5:1:1, 5:1:1.2, and 5:1.5:1) with the same sand content under the same inlet pressure (1.4 MPa) were compared, and the comparison results are shown in Figure 8.

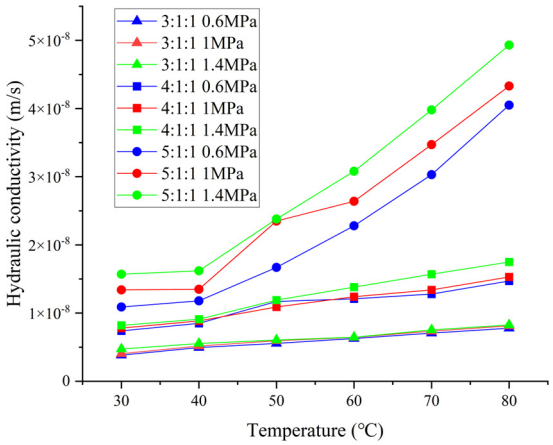

Figure 5. The hydraulic conductivity variety graph of the first group of rock samples (ratio X:1:1).

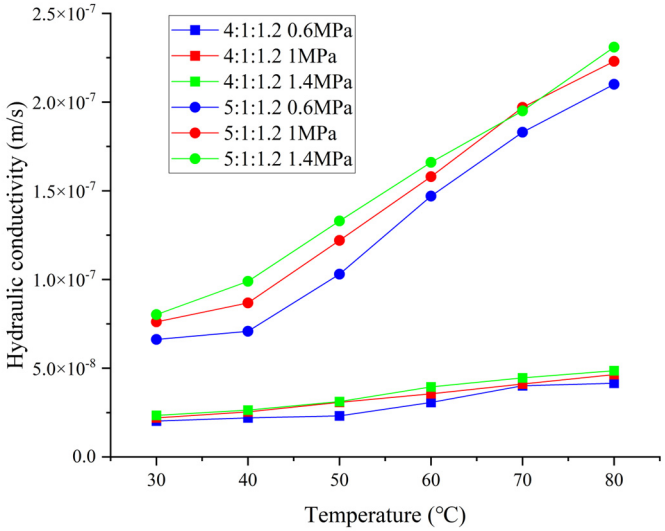

Figure 6. The hydraulic conductivity variety graph of the second group of rock samples (ratio X:1:1.2).

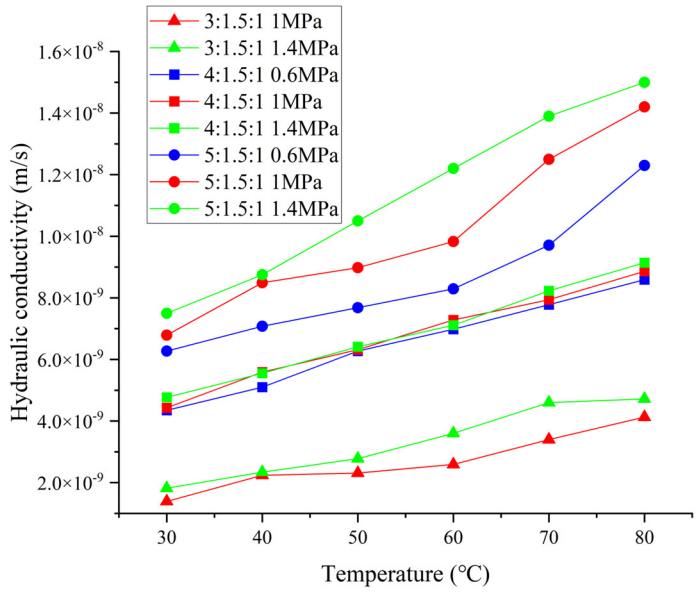

Figure 7. The hydraulic conductivity variety graph of the third group of rock samples (ratio X:1.5:1).

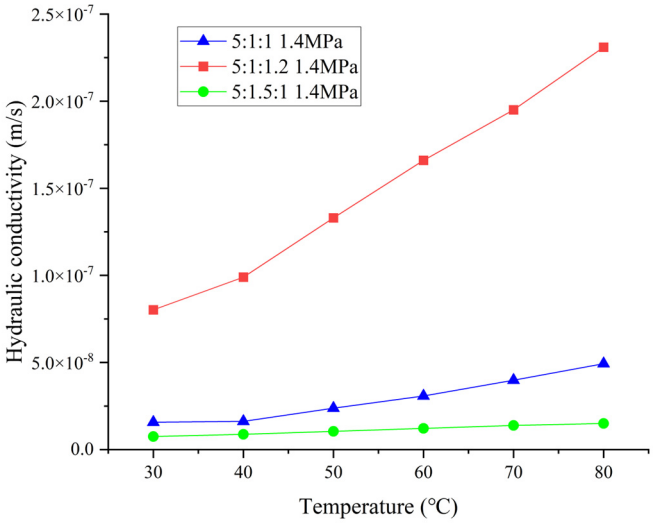

Figure 8. The hydraulic conductivity variety graph of rock samples with different ratios and the same sand content under the same inlet pressure (1.4 MPa) (ratio 5:X:X).

3.2. Experimental Results of Rock Samples with Fractured Media

The results of the above three groups of rock samples show that under different inlet pressures, the hydraulic conductivity increases with an increase in temperature. Considering that in the above experiments, the permeability path of water in the rock samples was all through the pores generated by fine sand consolidation, to verify the applicability of temperature to fractured rock mass, another rock sample with a ratio of 3:1:1 was selected after the above three groups of experiments. In the production process, thin steel sheets were put in when it was just cemented and withdrawn when it was about to set. In the process, damage to rock samples is avoided as much as possible, and fractures are taken into account. The rest of the installation and testing process was the same as before, and finally, two groups of artificially made rock samples containing fractures were obtained. The permeability test of the two groups of rock samples under different inlet pressures and varying temperature were carried out, and the hydraulic conductivity change was compared with the initial rock samples of the ratio (L = 0 cm), and the results were obtained, as shown in Figure 9:

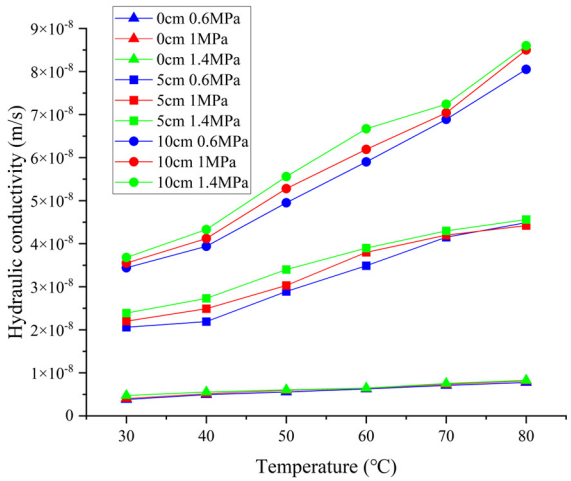

Figure 9. The hydraulic conductivity variety graph of the fractured rock samples.

3.3. Results Analysis

Through testing the hydraulic conductivity changes of porous rock samples at different temperatures and pressures in the early stage of the experiment, combined with the two supplementary groups of fractured rock samples, the following rules were finally obtained:

1. The difference between the porosity of rock samples at 30 °C and 80 °C was between 1–6% (Table 1), which indicates that the internal porosity of rock samples is good within the normal range. Compared with the artificial rock samples, the porosity of field rock samples was correspondingly much smaller. Due to the buried depth of nearly 1000 m, the sandstones in the original samples were subjected to greater confining pressure, generally dozens of MPa, the deposition activity was long, and the internal pores of the rock were compacted to a high degree.
2. The overall hydraulic conductivity of rock samples with different ratios increases with an increase in temperature. The growth rate was different in different temperature ranges, and there was a significant increase in the range of 40–50 °C (Figures 5–7). Considering that the rock properties changed little at low temperatures, the obvious increase of hydraulic conductivity should have been caused by the change of some parameters of water with the change in water temperature.
3. In the temperature range set in this experiment, the hydraulic conductivity at the highest temperature was significantly different from that at the lowest temperature,

and the variation range was 2–3 times. Moreover, there was also a correlation between hydraulic conductivity and inlet pressures provided by the pressure pump, which generally shows that the permeability under higher pressure conditions is stronger than that under lower pressure conditions (Figures 5–7). It is considered that due to the increase in pressure, the penetration rate of the water was accelerated, and strong water pressure may have affected the seepage mechanism in the rock samples, thus widening the water channel; however, the influence of water inlet pressures was relatively small.

4. According to the experimental design, the rock samples with different water–cement ratios were tested, and the expected effect was achieved. By comparing the three groups of rock samples (Figure 8) with the first group of rock samples, the water content in the water–cement ratio increased in the second group of rock samples. Relatively more cement participated in cementation, which was favorable for the formation of water channels, and the hydraulic conductivity was increased on the whole. Compared with the first group, due to the increase in cement content in the water–cement ratio, the cementation degree of the third group of samples was increased, the internal density degree was higher, and the overall hydraulic conductivity was decreased.
5. When the artificial fracture factor is added to the supplementary rock samples, the seepage form inside the rock samples will change, but the regularity of the final results was the same as the previous three groups of rock samples, which all show that the hydraulic conductivity increases with the increase in temperature. It can be considered that the influence of temperature on the permeability of rock samples is independent of the way of fluid penetration. By comparing the hydraulic conductivity of rock samples with different fracture lengths, when the fracture L = 10 cm of the rock sample, the tested hydraulic conductivity was larger than that of the rock sample with L = 5 cm, and when the fracture L = 5 cm, the hydraulic conductivity was larger than that of the conventional rock sample (Figure 9), indicating that the lengthening of the fracture extends the flow channel of seepage in the fracture. Moreover, it is easier to flow in fractures than in pores, so the permeability capacity of the rock samples becomes stronger with the growth of fractures.

4. Results of Numerical Simulation

4.1. Calculation Results

In this experiment, the changes in permeability parameters with temperature under different inlet pressures were simulated. During the simulation, it was found that the change in inlet pressure will not cause a variation in the hydraulic conductivity with temperature, which is well understood since the hydraulic conductivity of the rock mass is a function of density and viscosity, and when the density and viscosity are determined as a function of temperature, the hydraulic conductivity is determined, independent of the water injection pressure; however, will cause a change in Darcy's seepage velocity (Figure 10). This phenomenon has been observed in laboratory experiments; the change in inlet pressures does not significantly cause a change in hydraulic conductivity.

In the simulation process, it was noted that different water inlet pressures had an effect on the heating process of rocks. Figure 11 shows the temperature rise of rock mass under different injection pressures at 300 min.

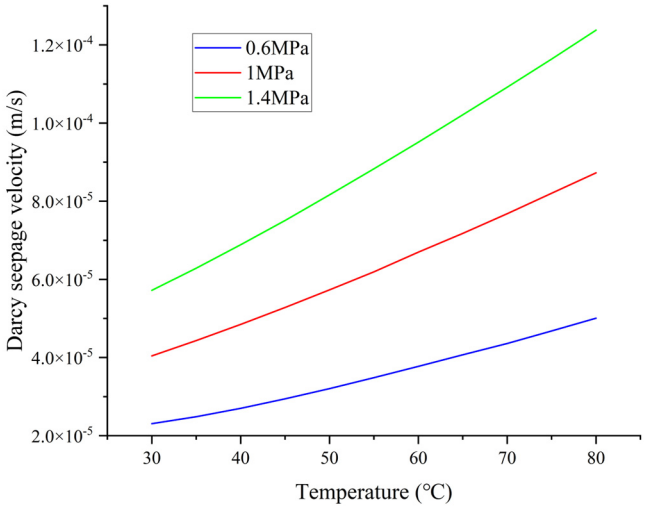

Figure 10. The Darcy seepage velocity with temperature variety graph under different inlet pressures.

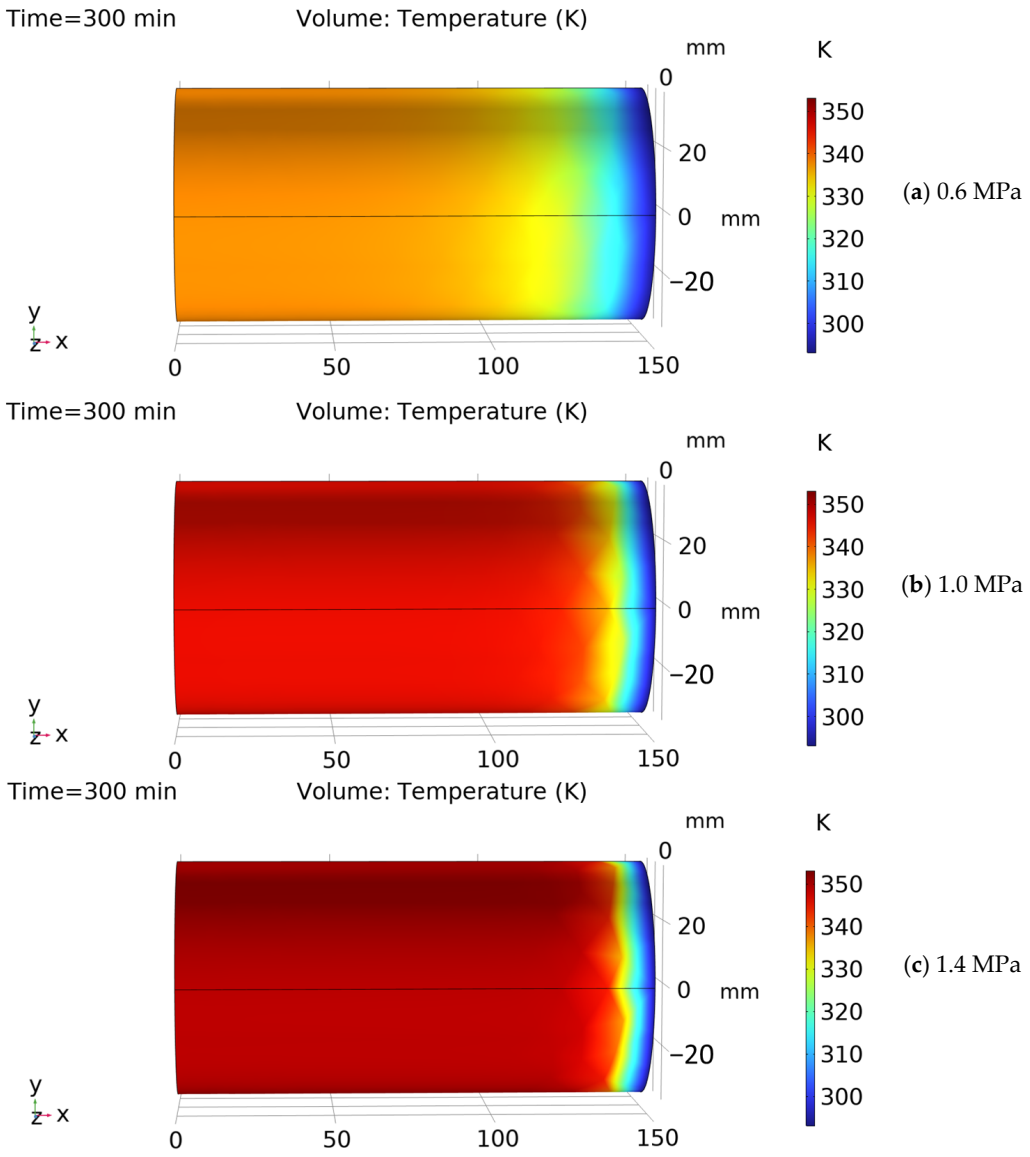

Figure 11. Rock temperature at 300 min under different water inlet pressures.

The time required for the monitoring point of rock to be heated to the corresponding temperature varies with the inlet pressures. Figure 12 shows the temperature change of

the monitoring point when the external heating temperature is 80 °C. At 600 min, the temperature of the rock basically reaches the external heating temperature. The initial conditions of the three curves only change the inlet pressures, and other parameters do not change.

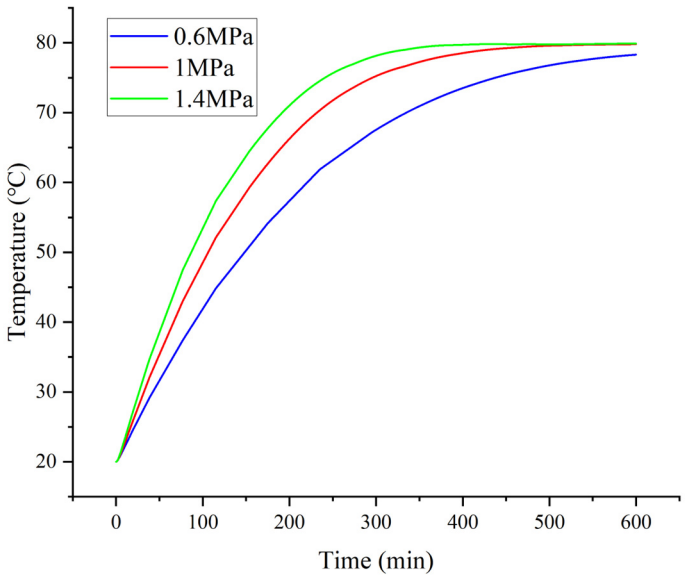

Figure 12. Time for the monitoring points to heat up to 80 °C at different inlet pressures.

4.2. Calculation Results Analysis

Combined with the actual geological background of the Zhaolou coal mine, on the basis of the laboratory experiment, the influence of water temperature change on Darcy's seepage velocity and hydraulic conductivity under different inlet pressures was numerically simulated by using the multi-physics coupling finite element software (COMSOL Multiphysics 5.6), and the same rules were obtained as in the laboratory experiment:

1. The hydraulic conductivity increases with the temperature. In the simulation process, it was found that the change in inlet pressures had no effect on the hydraulic conductivity, which was found in the laboratory experiment (Figures 5–7). In the laboratory experiment, the change in inlet pressures caused little variation in the hydraulic conductivity. It may be that the increase of water pressure in the laboratory experiment widened the water channel of the rock samples, but the porosity did not change with the change of inlet pressures in the numerical simulation, so this change cannot be reflected in the numerical simulation.
2. Darcy seepage velocity increases with the temperature and also with the inlet pressures (Figure 10). It is well understood that both temperature and pressure contribute to hydrodynamic strengthening. However, the increase in inlet pressure causes the increase in Darcy's seepage velocity but does not change the hydraulic conductivity, which is related to the boundary conditions set in this simulation. When the outlet pressure is 0, the hydraulic slope will increase with the increase in inlet pressure. According to Equation (2), the increase in hydraulic slope will cause an increase in seepage velocity. However, the seepage velocity will increase with the increase of water temperature. When the inlet pressure is unchanged, its hydraulic gradient is unchanged, and the reason for the seepage velocity increasing is the increase in its hydraulic conductivity. Therefore, the hydraulic conductivity and Darcy's seepage velocity show the same trend as the water temperature. To sum up, the hydraulic conductivity depends on the physical properties of the rock itself and the parameters related to the water temperature, while the seepage velocity has more hydraulic slope

influence than the hydraulic conductivity, so the two may not necessarily change simultaneously.

3. Under different inlet pressures, the time required to reach the same temperature for the monitoring point is different (Figure 10), and the increase in inlet pressure will cause an acceleration of Darcy's percolation velocity, so it is likely that water flow acts as the carrier of heat. The faster the seepage rate, the shorter the time required for heat to reach the monitoring point from the inlet, and therefore, the faster the heating rate, until finally, it reaches the same temperature as the external heating temperature and water temperature. Chai [29] studied the influence of seepage field on the temperature of concrete dams with porous media and obtained the basic equation as follows:

$$\frac{\partial}{\partial x}\left(\lambda c\frac{\partial T}{\partial x}\right) - c_w\rho_w\frac{\partial(v_x T)}{\partial x} + Q_T = c_c\rho_c\frac{\partial T}{\partial x} \tag{4}$$

where c_w is the specific heat of water ($\frac{w}{m}\cdot k$), ρ_w is the water density ($\frac{Kg}{m^3}$), Q_T is the exchange heat (J), v_x is the seepage velocity ($\frac{m}{s}$), c_c is the specific heat of porous media ($\frac{w}{m}\cdot k$), ρ_c is the porous media density ($\frac{Kg}{m^3}$), T is the temperature (°C), and λc is a constant.

It can be seen from Equation (4) that the seepage velocity will affect the heat exchange velocity and thus affect the temperature change trend with time. Therefore, Equation (4) can well explain the difference in the temperature rise trend of the monitoring points in Figure 10.

5. Discussion

5.1. Analysis of Influencing Hydraulic Conductivity of Rock Samples with Different Ratios

The laboratory experiment results have proven that the hydraulic conductivity increases significantly with the sand content, and the changing trend is more obvious with the change in temperature. However, the increase in sand content of rock samples does not greatly improve the porosity of the rock (Table 1). Therefore, the increasing porosity is not the direct reason for the hydraulic conductivity change caused by the sand content. It is more likely that the increase and change in sand content make the connectivity of the internal pores better, thus forming a path more conducive to water flow. Ahmad and Azad [30] found in the permeability experiment of concrete with the same porous media that porosity itself could not determine the hydraulic conductivity of rock samples, and according to Equation (5), its hydraulic conductivity was more dependent on the ratio of concrete porosity ($\mathcal{E}$) to tortuosity (τ). Moreover, Ahmad and Azad [30] found that there was a positive correlation.

$$K = c_0\left(\frac{\varepsilon}{\tau}\right)\left(\frac{\varepsilon}{M_S(1-\varepsilon)}\right)^2\left(\frac{g}{v}\right) \tag{5}$$

where K is the hydraulic conductivity (m/s), c_0 is a constant, $\mathcal{E}$ is the porosity, τ is the tortuosity, Ms is the specific surface, g is the acceleration of gravity (m/s^2), and v is the kinematic viscosity (m^2/s).

The relationship between the hydraulic conductivity and the tortuosity of porous media has been proved by many studies [31,32], combined with the small change in porosity, and the tortuosity of porous media will change with a change in the water–cement ratio [30,33]; therefore, the obvious increase of rock hydraulic conductivity with sand content in this paper may be caused by the decrease in the tortuosity of the sandstone, but further research is still needed.

Similarly, Table 1 shows that a change in cement content will cause certain changes in porosity, but as mentioned above, the ratio of porosity to tortuosity is more correlated with a change in hydraulic conductivity, so it can also be used to understand the change in hydraulic conductivity caused by the change in cement and water content. In terms of the

mechanism, the increase in cement content will make the degree of cementation between rock pores better and inhibit the connectivity between pores, thus blocking the water channel and causing a decrease in the hydraulic conductivity of rock samples. However, an increase in water brings the opposite result, which makes the pore cementation between the pores of the rock deteriorate and leads to an increase in the hydraulic conductivity of the rock samples.

To sum up, the change in hydraulic conductivity of rock samples with different ratios is not caused by the single factor of porosity but by changes to multiple parameters. From the perspective of internal mechanisms, the change in parameters causes the change in pore connectivity, forming or blocking the flow channel. Compared with the porous media, the hydraulic conductivity of the fractured rock samples in Figure 6 is larger, and the fractured rock samples have a more favorable fracture channel for water flow.

5.2. The Relationship Between Temperature and Hydraulic Conductivity

As can be seen from Table 1, the porosity of rocks at 80 °C is not much different from that at 30 °C. Moreover, the permeability experiment is conducted at 30–80 °C, and at this low temperature, the internal structure of the rocks generally does not change (generally, the internal structure of rocks will change at 400 °C) [34,35]; therefore, the hydraulic conductivity increase should not be caused by the temperature change in pore connectivity, so it is more likely that the physical properties of water changing at high temperature has an impact on the hydraulic conductivity. The influence of the kinematic viscosity of water on hydraulic conductivity should not be ignored [36,37]; the hydraulic conductivity in isotropic media is defined as the unit flow rate under the unit hydraulic gradient indicating the difficulty of fluid through the pore skeleton, and the expression is as follows:

$$K = \frac{gk}{v} \tag{6}$$

where K is the hydraulic conductivity (m/s), g is the acceleration of gravity (m/s^2), k is the permeability (m^2), and v is the kinematic viscosity (m^2/s).

Fluid viscosity varies with temperature [38] and accordingly affects relative hydraulic conductivity [39,40], and according to the empirical formula [41], the relationship between the kinematic viscosity v of water and temperature is as follows:

$$v = \frac{0.01775}{1 + 0.033T + 0.000221T^2} \tag{7}$$

where T is the temperature of water (°C) and v is the kinematic viscosity (m^2/s).

By substituting Equation (7) into Equation (6), the following equation can be obtained:

$$K = \frac{gk}{0.01775}\left(1 + 0.033T + 0.000221T^2\right) \tag{8}$$

In Table 1, the porosity of artificial rock samples at high temperatures is not much different from that at normal temperatures, ranging from 1–6%, so the permeability of porous media changes little, parameter k in Equation (8) changes little, and thus it can be equated to a constant. In Equation (8), g and k have a constant value, so K only changes with the change of T. The hydraulic conductivity of rocks at 80 °C and 30 °C is compared as follows:

$$\frac{K(80)}{K(30)} = 2.31 \tag{9}$$

According to the laboratory experiment, the artificial rock sample of 3:1.5:1 has the highest similarity with the fine sandstone in the real rock, and the data obtained in the

permeability measurement experiment of this rock sample are fitted with the similarity in relevant software (Figure 13).

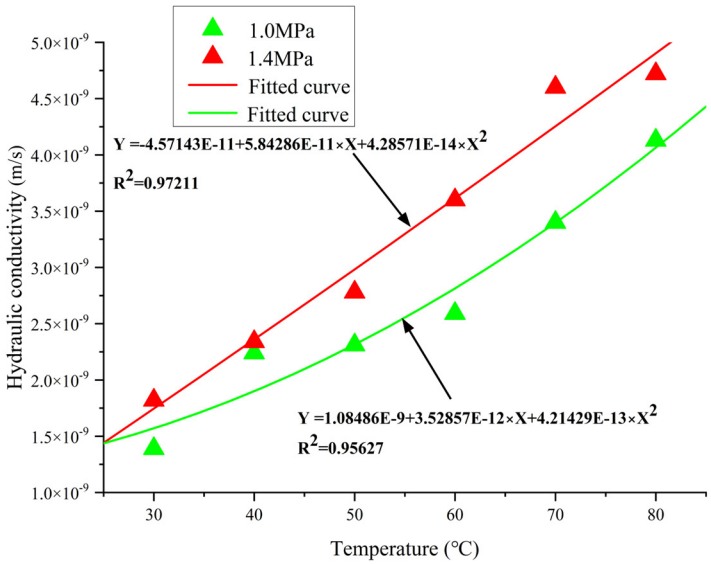

Figure 13. The fitting result of the artificial rock sample with the ratio of 3:1.5:1.

Figure 13 shows that the hydraulic conductivity of the artificial rock sample with the ratio of 3:1.5:1 shows a change rule similar to that of Equation (8) after fitting. The fitting equation shows that the corresponding value of rock samples with different ratios will also be different, indicating the difference in permeability of rock samples with different ratios. At the same time, the hydraulic conductivity of the 3:1.5:1 rock sample at 80 °C is 2.27 times higher than that tested at 30 °C, which is very consistent with the theoretical analysis. The results of this experiment are explained from the perspective of the influence of temperature on the physical properties of water, and it is believed that the influence of temperature on the hydraulic conductivity of rock is as follows: it is mainly reflected in the influence on the kinematic viscosity of water, which manifests as an increase in the hydraulic conductivity of rock samples.

5.3. Influence of Temperature on Mine Water Inflow

Through the previous analyses, the temperature increases will cause the kinematic viscosity of water to decrease, and the hydraulic conductivity will increase accordingly; the change in the hydraulic conductivity of the deep aquifer will lead to a change in the water inflow in coal mining. Therefore, the analytical method was used to predict the water inflow in Zhaolou Coal Mine, and according to Equation (9), the hydraulic coefficient of the aquifer was corrected to compare the difference of the water inflow in the mine at the temperature of 30 °C and 80 °C.

According to the comprehensive analysis of the hydrogeological conditions of the Zhaolou Coal Mine, the top and bottom sandstones of the No. 3 coal seam and the No. 3 limestones of the Taiyuan Formation are the direct water-filled aquifers for mining the No. 3 coal seam. Therefore, it can be assumed that these two aquifers constitute the normal water inflow of the mine.

According to the analysis and generalization of hydrogeological conditions in Zhaolou Coal Mine, the prediction of the water inflow in the top and bottom sandstones is expected to use the following stable-flow infinite-boundary pressurized–unpressurized formula:

$$Q_1 = 1.366K\frac{(2s - M)M - h^2}{\log R_0 - \log r_0} \quad (10)$$

$$R = 10s\sqrt{K} \tag{11}$$

$$r_0 = \sqrt{F/\pi} \tag{12}$$

$$R_0 = R + r_0 \tag{13}$$

where Q_1 is the water inflow in the top and bottom sandstones of the No. 3 coal seam (m^3/h), M is the thickness of the aquifer (m), s is the water level drawdown value (m), h is the dynamic water level (m), K is the permeability coefficient (m/d), F is the generalized area (m^2), R is the radius of influence (m), r_0 is the quoted radius (m), and R_0 is the quoted radius of influence (m).

In the calculation of the No. 3 limestones of the Taiyuan Formation water inflow, taking into account the calculated radius of influence is much larger than the Zhaolou Coal Mine Tianqiao Fault, so the fault will be generalized to a straight line of waterproof boundary, using a straight line of waterproof boundary pressurized water formula as follows:

$$Q_2 = \frac{2.73KMs}{R_A} \tag{14}$$

$$R_A = \log\frac{R_0^2}{2br_0} \tag{15}$$

where b is the distance from the waterproof boundary (m).

The relevant parameters are brought into the above formula, and the water inflow volume of two aquifers under the temperature of 30 °C and 80 °C are calculated respectively, and the results are shown in Table 3:

Table 3. Water inflow at two temperatures.

Water Inflow (m^3/h)	30 °C	80 °C	Amplitude
No. 3 coal seam top and bottom sandstone water inflow	174.2	296.4	170.1%
No. 3 limestone water inflow	166.0	345.1	207.9%
Mine water inflow	340.3	641.4	188.5%

Comparing the above two temperatures of mine water inflow, we have found that when the underground temperature changes to 80 °C, the predicted water inflow volume of ZhaoLou Coal Mine at 30 °C increased by 301.2 m^3/h, an increase of 188.5%, indicating that the underground temperature is an important factor affecting the water inflow in the mine.

According to Equations (7) and (8), the temperature increases will cause the kinematic viscosity of water to decrease, and the hydraulic conductivity of water increases accordingly. This has been verified by experiments of many scholars [15,27], but these experiments are usually fractured rock mass after high-temperature heat treatment, which is of great significance for deep geothermal development. In this paper, taking Zhaolou Coal Mine deep mining as the actual geological background, the hydraulic conductivity of water with variable temperatures was studied by artificially expanding the porosity under relatively low-temperature conditions. The change in hydraulic conductivity of deep aquifers will cause water inrush disasters in coal mining. The research insights of this paper have great practical significance for deep mining, such as coal mining.

6. Conclusions

Based on the background of deep coal mining, the hydraulic conductivity of rock samples of different components is simulated and tested under different temperatures and water pressures through the self-designed experimental apparatus. Finally, the coupling

relationship between the temperature field and the seepage field was discussed through multi-physical field coupling analysis, and the laboratory experiment was well verified. The main conclusions are as follows:

1. In the temperature range of 30~80 °C, it was found that the hydraulic conductivity of similar-material rock samples showed an increasing trend with the temperature, which was also correlated with the different ratios of the materials. Overall, an increase in water–sand content and a decrease in cement content lead to an increase in hydraulic conductivity. At the same time, the fractured rock samples with the same ratio have stronger permeability than the rock sample without fractures.
2. The coupling numerical model of the seepage field and temperature field found that the seepage velocity and hydraulic conductivity have a certain synchronization with the change in temperature, but there is a hydraulic slope in the influencing factors of seepage velocity.
3. The relationship between temperature and hydraulic conductivity is discussed. The kinematic viscosity decreases with the increase in temperature, which is conducive to the flow of fluid in rocks. Further calculations proved that higher temperature water leads to higher hydraulic conductivity and ultimately increases the mine water inflow, proving that temperature is an important factor in the increase of water inrush in deep coal mining.

Author Contributions: Conceptualization, H.Q. and S.Z.; Data curation, X.L.; Investigation, H.Q. and H.F.; Methodology, H.Q.; Supervision, S.Z.; Writing—original draft, H.Q.; Writing—review and editing, S.Z. All authors have read and agreed to the published version of the manuscript.

Funding: This work was funded by the National Natural Science Foundation of China (Grant No. 52274243).

Data Availability Statement: The data that support the findings of this study are available on request from the corresponding author.

Acknowledgments: The authors are grateful to the editors and anonymous reviewers for their helpful comments on the manuscript.

Conflicts of Interest: The authors have not disclosed any competing interests.

References

1. Li, Q.; Li, Q.C.; Wang, F.L.; Wu, J.J.; Wang, Y.L. The Carrying Behavior of Water-Based Fracturing Fluid in Shale Reservoir Fractures and Molecular Dynamics of Sand-Carrying Mechanism. *Processes* **2024**, *12*, 2051. [CrossRef]
2. Li, Q.C.; Li, Q.; Han, Y. A Numerical Investigation on Kick Control with the Displacement Kill Method during a Well Test in a Deep-Water Gas Reservoir: A Case Study. *Processes* **2024**, *12*, 2090. [CrossRef]
3. He, M.C.; Xie, H.P.; Peng, S.P. Study on rock mechanics in deep mining engineering. *Chin. J. Rock Mech. Eng.* **2005**, 2803–2813.
4. Zhang, Z.; Zhang, Q.; Duan, K.; Zhang, R.; Lin, H.; Xiang, W. A fully coupled hydraulic-mechanical model of deep tunnel considering permeability variation. *Comput. Geotech.* **2022**, *151*, 104984. [CrossRef]
5. Song, Z.; Zhang, J. Progressive failure mechanical behaviour and response characteristics of sandstone under stress-seepage coupling. *J. Geophys. Eng.* **2021**, *18*, 200–218. [CrossRef]
6. Yang, T.H.; Jia, P.; Shi, W.H.; Wang, P.T.; Liu, H.L.; Yu, Q.L. Seepage–stress coupled analysis on anisotropic characteristics of the fractured rock mass around roadway. *Tunn. Undergr. Space Technol.* **2014**, *43*, 11–19. [CrossRef]
7. Zhang, J.-w.; Song, Z.-x.; Wang, S.-y. Mechanical behavior of deep sandstone under high stress-seepage coupling. *J. Cent. South Univ.* **2021**, *28*, 3190–3206. [CrossRef]
8. Frank, S.; Heinze, T.; Pollak, S.; Wohnlich, S. Transient heat transfer processes in a single rock fracture at high flow rates. *Geothermics* **2021**, *89*, 101989. [CrossRef]
9. Liu, X.; Zeng, Y.; Wu, Q.; Meng, S.; Liang, J.; Hou, Z. Ecological-Based Mining: A Coal–Water–Thermal Collaborative Paradigm in Ecologically Fragile Areas in Western China. *Engineering* **2024**, *38*, 209–222. [CrossRef]

10. Luo, S.; Zhao, Z.; Peng, H.; Pu, H. The role of fracture surface roughness in macroscopic fluid flow and heat transfer in fractured rocks. *Int. J. Rock Mech. Min. Sci.* **2016**, *87*, 29–38. [CrossRef]
11. Ji, Z.; Tian, H.; Yang, Z.; Liu, T.; Bandara, S.; Sundhararajan, M.; Gao, X.-Z.; Vahdat Nejad, H. Mechanism of water inrush from coal seam floor based on coupling mechanism of seepage and stress. *J. Intell. Fuzzy Syst.* **2018**, *34*, 965–974. [CrossRef]
12. Pan, Y.; Wang, H.; Liu, Q. Coupled Hydraulic-Thermal Modelling and Related Numerical Analysis on Rock Fractures. *Geofluids* **2020**, *2020*, 8830862. [CrossRef]
13. Yan, C.; Xie, X.; Ren, Y.; Ke, W.; Wang, G. A FDEM-based 2D coupled thermal-hydro-mechanical model for multiphysical simulation of rock fracturing. *Int. J. Rock Mech. Min. Sci.* **2022**, *149*, 104964. [CrossRef]
14. Ji, Y.; Xu, H.; Zhang, J.; Guo, L. Analytical modeling on the geo-stress and casing damage prevention with the thermo-hydro-mechanical (THM) coupling of multi-field physics. *J. Therm. Anal. Calorim.* **2019**, *139*, 2719–2737. [CrossRef]
15. Luo, J.; Zhu, Y.; Guo, Q.; Tan, L.; Zhuang, Y.; Liu, M.; Zhang, C.; Xiang, W.; Rohn, J. Experimental investigation of the hydraulic and heat-transfer properties of artificially fractured granite. *Sci. Rep.* **2017**, *7*, 39882. [CrossRef]
16. Shi, Z.; Yao, Q.; Wang, W.; Su, F.; Li, X.; Zhu, L.; Wu, C. Size Effects of Rough Fracture Seepage in Rocks of Different Scales. *Water* **2023**, *15*, 1912. [CrossRef]
17. Wang, W.; Faybishenko, B.; Jiang, T.; Dong, J.; Li, Y. Seepage Characteristics of a Single Ascending Relief Well Dewatering an Overlying Aquifer. *Water* **2020**, *12*, 919. [CrossRef]
18. Liu, G.; Zhao, Z.; Chen, Y.; Ma, F.; Wang, G. Comparison between typical numerical models for fluid flow and heat transfer through single rock fractures. *Comput. Geotech.* **2021**, *138*, 104341. [CrossRef]
19. Min, K.-B.; Rutqvist, J.; Tsang, C.-F.; Jing, L. Thermally induced mechanical and permeability changes around a nuclear waste repository—A far-field study based on equivalent properties determined by a discrete approach. *Int. J. Rock Mech. Min. Sci.* **2005**, *42*, 765–780. [CrossRef]
20. Chen, L.; Li, J.; Zhang, Y.; Han, F.; Ji, C.; Zhang, J. Study on coupled heat transfer and seepage in large sparsely fractured surrounding rocks in deep underground spaces. *Appl. Therm. Eng.* **2019**, *162*, 114277. [CrossRef]
21. Li, Z.; Zhou, Z. Numerical Simulation of Rock Fracture and Permeability Characteristics under Stress–Seepage–Damage Coupling Action. *Int. J. Geomech.* **2023**, *23*, 04022257. [CrossRef]
22. Li, Z.-h.; Feng, G.-r.; Zhai, C.-z. Study on "triangle" water-inrush mode of strong water-guide collapse column. *J. Cent. South Univ.* **2016**, *23*, 2402–2409. [CrossRef]
23. Teng, T.; Li, Z.; Wang, Y.; Liu, K.; Jia, W. Experimental and Numerical Validation of an Effective Stress-Sensitive Permeability Model Under Hydromechanical Interactions. *Transp. Porous Media* **2024**, *151*, 449–467. [CrossRef]
24. Khlapuk, M.M.; Klimov, S.V.; Bezusiak, O.V.; Shumlyanskyi, A.O. Experimental study of the effect of hydraulic gradient on soil hydraulic conductivity. *IOP Conf. Ser. Earth Environ. Sci.* **2024**, *1415*, 012090. [CrossRef]
25. Güneri, E.; Yukselen-Aksoy, Y. Volume Deformation and Hydraulic Conductivity Behavior of Sand-Bentonite Mixtures with Fiberglass Additives under High Temperatures. *J. Mater. Civ. Eng.* **2024**, *36*, 04024021. [CrossRef]
26. Zeng, Y.; Mei, A.; Wu, Q.; Meng, S.; Zhao, D.; Hua, Z. Double verification and quantitative traceability: A solution for mixed mine water sources. *J. Hydrol.* **2024**, *630*, 130725. [CrossRef]
27. Shu, B.; Zhu, R.; Tan, J.; Zhang, S.; Liang, M. Evolution of permeability in a single granite fracture at high temperature. *Fuel* **2019**, *242*, 12–22. [CrossRef]
28. Gray, W.G.; Miller, C.T. Examination of Darcy's Law for Flow in Porous Media with Variable Porosity. *Environ. Sci. Technol.* **2004**, *38*, 5895–5901. [CrossRef]
29. Chai, J. Analysis of coupled seepage and temperature fields in concrete dam. *Commun. Numer. Methods Eng.* **2002**, *18*, 399–409. [CrossRef]
30. Ahmad, S.; Azad, A.K. An exploratory study on correlating the permeability of concrete with its porosity and tortuosity. *Adv. Cem. Res.* **2013**, *25*, 288–294. [CrossRef]
31. Graczyk, K.M.; Strzelczyk, D.; Matyka, M. Deep learning for diffusion in porous media. *Sci. Rep.* **2023**, *13*, 9769. [CrossRef] [PubMed]
32. Kimura, M. Prediction of tortuosity, permeability, and pore radius of water-saturated unconsolidated glass beads and sands. *J. Acoust. Soc. Am.* **2018**, *143*, 3154–3168. [CrossRef]
33. Cardoso, R. Porosity and tortuosity influence on geophysical properties of an artificially cemented sand. *Eng. Geol.* **2016**, *211*, 198–207. [CrossRef]
34. Sun, Q.; Zhang, W.; Su, T.; Zhu, S. Variation of Wave Velocity and Porosity of Sandstone after High Temperature Heating. *Acta Geophys.* **2016**, *64*, 633–648. [CrossRef]
35. Zhang, Y.; Sun, Q.; He, H.; Cao, L.; Zhang, W.; Wang, B. Pore characteristics and mechanical properties of sandstone under the influence of temperature. *Appl. Therm. Eng.* **2017**, *113*, 537–543. [CrossRef]

36. Fan, M.; Dalton, L.E.; McClure, J.; Ripepi, N.; Westman, E.; Crandall, D.; Chen, C. Comprehensive study of the interactions between the critical dimensionless numbers associated with multiphase flow in 3D porous media. *Fuel* **2019**, *252*, 522–533. [CrossRef]
37. Xiong, F.; Sun, W.; Ba, J.; Carcione, J.M. Effects of Fluid Rheology and Pore Connectivity on Rock Permeability Based on a Network Model. *J. Geophys. Res. Solid Earth* **2020**, *125*, e2019JB018857. [CrossRef]
38. Seeton, C.J. Viscosity–temperature correlation for liquids. *Tribol. Lett.* **2006**, *22*, 67–78. [CrossRef]
39. Balogun, Y.; Iyi, D.; Faisal, N.; Oyeneyin, B.; Oluyemi, G.; Mahon, R. Experimental investigation of the effect of temperature on two-phase oil-water relative permeability. *J. Pet. Sci. Eng.* **2021**, *203*, 108645. [CrossRef]
40. Li, H.; Pan, C.; Miller, C.T. Pore-scale investigation of viscous coupling effects for two-phase flow in porous media. *Phys. Rev. E* **2005**, *72*, 026705. [CrossRef] [PubMed]
41. Yu, C.Z. *Introduction to Environmental Fluid Mechanics*; Tsinghua University Press: Beijing, China, 1992.

Disclaimer/Publisher's Note: The statements, opinions and data contained in all publications are solely those of the individual author(s) and contributor(s) and not of MDPI and/or the editor(s). MDPI and/or the editor(s) disclaim responsibility for any injury to people or property resulting from any ideas, methods, instructions or products referred to in the content.